Cytopathic effects of the cytomegalovirus-encoded apoptosis inhibitory protein vMIA

Delphine Poncet,[1] Anne-Laure Pauleau,[1] Gyorgy Szabadkai,[2] Angelo Vozza,[3] Sebastian R. Scholz,[3] Morgane Le Bras,[4] Jean-Jacques Brière,[5] Abdelali Jalil,[6] Ronan Le Moigne,[7] Catherine Brenner,[4] Gabriele Hahn,[8] Ilka Wittig,[9] Hermann Schägger,[9] Christophe Lemaire,[4] Katiuscia Bianchi,[2] Sylvie Souquère,[10] Gerard Pierron,[10] Pierre Rustin,[5] Victor S. Goldmacher,[11] Rosario Rizzuto,[2] Ferdinando Palmieri,[3] and Guido Kroemer[1]

[1]Centre National de la Recherche Scientifique, FRE2939, Institut Gustave Roussy, F-94805 Villejuif, France
[2]Department of Experimental and Diagnostic Medicine, Section of General Pathology, University of Ferrara, Ferrara 44100, Italy
[3]Department of Pharmaco-Biology, Laboratory of Biochemistry and Molecular Biology, University of Bari, 70125 Bari, Italy
[4]Centre National de la Recherche Scientifique, UMR8159, Université de Versailles-St. Quentin, 78035 Versailles Cedex, France
[5]Institut National de la Santé et de la Recherche Médicale U676, Hopital Robert Debré, 75019 Paris, France
[6]Service Commun de Microscopie Confocale, Institut Gustave Roussy, [7]UMR8113, ENS Cachan, 94230 Cachan
[8]Max von Pettenkofer Institut, Universitaet Muenchen, 80336 Muenchen, Germany
[9]Molekular Bioenergetik, Zentrum der Biologischen Chemie, Universätsklinikum Frankfurt, D-60590 Frankfurt, Germany
[10]Institut André Lwoff, UPR-1983, Laboratoire Replication de l'ADN et Ultrastructure du Noyau, 94801 Villejuif, France
[11]ImmunoGen Inc., Cambridge, MA 02139

Replication of human cytomegalovirus (CMV) requires the expression of the viral mitochondria–localized inhibitor of apoptosis (vMIA). vMIA inhibits apoptosis by recruiting Bax to mitochondria, resulting in its neutralization. We show that vMIA decreases cell size, reduces actin polymerization, and induces cell rounding. As compared with vMIA-expressing CMV, vMIA-deficient CMV, which replicates in fibroblasts expressing the adenoviral apoptosis suppressor E1B19K, induces less cytopathic effects. These vMIA effects can be separated from its cell death–inhibitory function because vMIA modulates cellular morphology in Bax-deficient cells. Expression of vMIA coincided with a reduction in the cellular adenosine triphosphate (ATP) level. vMIA selectively inhibited one component of the ATP synthasome, namely, the mitochondrial phosphate carrier. Exposure of cells to inhibitors of oxidative phosphorylation produced similar effects, such as an ATP level reduced by 30%, smaller cell size, and deficient actin polymerization. Similarly, knockdown of the phosphate carrier reduced cell size. Our data suggest that the cytopathic effect of CMV can be explained by vMIA effects on mitochondrial bioenergetics.

Introduction

Human cytomegalovirus (CMV) received its name from its capacity to induce two characteristic and successive cytopathic effects. The early cytopathic effect (ECE) consists of the rounding of infected fibroblasts, whereas the late cytopathic effect (LCE) is characterized by the appearance of granular or dense intracytoplasmic and intranuclear inclusion bodies, as well as by an increased cell volume (Gandhi and Khanna, 2004; Sekhon et al., 2004). The molecular mechanisms accounting for these cytopathic effects are elusive.

CMV is an opportunistic pathogen that establishes lifelong latent infection without overt clinical disease in immunocompetent individuals, but can cause severe illness in utero, in neonates, and in patients with acquired or iatrogenic immunodeficiency. CMV infection can be associated with colitis (Tzankov et al., 2003), retinitis (Chiou et al., 2002), and encephalitis (DeBiasi et al., 2002) accompanied by local cell deaths.

CMV encodes two antiapoptotic proteins, especially the viral mitochondria–localized inhibitor of apoptosis (vMIA; pUL37 × 1; Goldmacher et al., 1999). vMIA protects CMV-infected cells from apoptosis in the late phase of the viral life cycle (Reboredo et al., 2004), and thus, vMIA-deficient CMV cannot replicate (because it kills the infected cells) unless it infects cells that overexpress Bcl-2–like apoptosis inhibitors such

D. Poncet and A.-L. Pauleau contributed equally to this paper.

Correspondence to Guido Kroemer: kroemer@igr.fr

Abbreviations used in this paper: ANT, adenine nucleotide translocase; CMV, cytomegalovirus; EA, early antigen; ECE, early cytopathic effect; FSC, forward scatter channel; IEA, immediate early antigen; LCE, late cytopathic effect; MOMP, mitochondrial outer membrane permeabilization; PiC, phosphate inorganic carrier; RC, respiratory control; vMIA, viral mitochondria–localized inhibitor of apoptosis.

The online version of this article contains supplemental material.

The Journal of Cell Biology, Vol. 174, No. 7, September 25, 2006 985–996
http://www.jcb.org/cgi/doi/10.1083/jcb.200604069

as E1B19K (Reboredo et al., 2004). Although there is some functional similarity between Bcl-2 and vMIA, which both inhibit apoptosis-associated mitochondrial outer membrane permeabilization (MOMP), there is no obvious sequence similarity between the two proteins (Goldmacher et al., 1999; Boya et al., 2001, 2004; Hayajneh et al., 2001; Goldmacher, 2005). Moreover, in contrast to Bcl-2, vMIA induces the fragmentation of the tubular mitochondrial network, reducing its connectivity (McCormick et al., 2003; Perfettini et al., 2005). The vMIA protein is largely confined to the mitochondrial compartment, and it coimmunoprecipitates with the adenine nucleotide translocase (ANT; Goldmacher et al., 1999; Vieira et al., 2001), which is the antiporter responsible for the exchange of ADP and ATP at the inner mitochondrial membrane (for review see Palmieri, 2004). In addition, vMIA has been shown to physically interact with the protein Bax, recruiting it to mitochondria while neutralizing its proapoptotic function (Poncet et al., 2004). Because vMIA loses its antiapoptotic action in Bax-deficient cells (Arnoult et al., 2004), it appears that vMIA exerts its antiapoptotic function solely by neutralizing Bax.

Based on these premises, we decided to evaluate the contribution of vMIA to CMV-induced cytopathic effects. We report that vMIA mediates the ECEs and LCEs of CMV infection through a novel effect on mitochondrial bioenergetics that is independent from its antiapoptotic function.

Results

Effects of vMIA on mitochondrial morphology, cell size, actin cytoskeleton, and cellular dynamics

Mitochondria of two stable cell lines constitutively expressing vMIA, i.e., a human cervical carcinoma cell line (HeLa) and an immortalized mouse fibroblast cell line (NIH3T3), look rounder and smaller than control mitochondria (Fig. 1 A). They present a highly disturbed organization, with mitochondrial fragmentation, matrix swelling, and reduction of the number of cristae (Fig. 1 B). This phenotype is not associated with a reduction of global mitochondrial mass, as determined by staining of the mitochondria with the potential-independent dye MitoTracker green (Fig. 1 C). Moreover, the abundance of proteins from the respiratory chain was not altered by vMIA (Fig. 1 D). We observed a reduction in the size of vMIA-expressing cells. This applied to both the cellular volume (Fig. 2 A) and the cytoplasmic membrane surface (Fig. 2 B) as measured by flow cytometry, as well as to the mean contact surface area of adherent cells (Fig. 2 C). There was no difference in the cell cycle distribution between vector-only and vMIA-transfected HeLa cells (Fig. S1 A, available at http://www.jcb.org/cgi/content/full/jcb.200604069/DC1), and the difference in size between vMIA-expressing and control cells was found in both the G1 and the G2/M phases of the cell cycle (Fig. S1 B). vMIA-expressing cells showed an altered actin cytoskeleton with fewer stress fibers and poorly polymerized cortical actin (Fig. 2 D). vMIA-expressing NIH3T3 cells exhibited a significant delay in their adherence compared with vector-only–transfected control cells (Fig. 2 E). Moreover, vMIA-expressing NIH3T3 cells were less efficient in "wound healing" in vitro, meaning that they migrated less rapidly into a cell-free area of the culture substratum, which was generated by scratching the monolayer (Fig. 2 F). Similarly, vMIA-expressing HeLa cells exhibited a reduced motility, as determined by videomicroscopy (unpublished data).

Apoptosis-unrelated morphological effects of vMIA

The effects of vMIA on cellular morphology appear to be independent from its impact on apoptosis regulation, as indicated by two independent lines of evidence. As compared with Neo cells, HeLa cells expressing vMIA were resistant against a panel of apoptosis inducers, including CD95 ligand, the lysosomal toxin ciprofloxacin (Boya et al., 2003), and anoikis. In contrast, vMIA had no apoptosis-inhibitory effects in NIH3T3 cells (Fig. S2, available at http://www.jcb.org/cgi/content/full/jcb.200604069/DC1). Thus, the vMIA effects on NIH3T3 cell morphology must be independent from its apoptosis-regulatory function. Accordingly, the siRNA-mediated knockdown of Bax, which is the target of vMIA-mediated apoptosis modulation (Arnoult et al., 2004; Poncet et al., 2004), did not reduce the size difference between Neo and vMIA-transfected HeLa cells (Fig. 3 A). siRNA-mediated knockdown of the Bax homologue Bak, which does not interact with vMIA (Arnoult et al., 2004), also failed to affect the size of vMIA-expressing cells (Fig. 3 B). Transient transfection of vMIA imposed a cell-size reduction accompanied by a transition from a filamentous to a punctate mitochondrial morphology in both $HCT116^{Bax+/-}$ cells, which express Bax, and $HCT116^{Bax-/-}$ cells, in which *Bax* was removed (Fig. 3, C and D). Altogether, these data provide strong evidence that the morphological effects of vMIA are independent from its apoptosis-inhibitory, Bax-mediated function.

Actin polymerization and migration properties of vMIA-expressing cells

Both control and vMIA-expressing HeLa cells were enlarged when plated on either collagen type I– or fibronectin-coated tissue plates, which increase adhesion to the culture substratum, but the difference in size between the cell types persisted (Fig. S3, available at http://www.jcb.org/cgi/content/full/jcb.200604069/DC1), pointing to an intrinsic metabolic alteration imposed by vMIA.

Actin rearrangements that occur during migration are mainly controlled by the Rho-GTPase family (Ridley, 2001; Raftopoulou and Hall, 2004). To check if these pathways were impaired in vMIA cells, we transfected HeLa cells with GFP-coupled wild-type RhoA and Rac-GTPase or with mutant constitutively activated GTPase Rho- and Rac-Q. The distribution of actin was not influenced by Rho-WT or Rac-WT, neither in control nor in vMIA-expressing cells (Fig. S4 A, available at http://www.jcb.org/cgi/content/full/jcb.200604069/DC1). This demonstrated that the vMIA-induced defect in actin polymerization (and hence in migration) was not secondary to a defect in Rho-GTPase function. The percentage of cells showing enhanced stress fiber polymerization in response to Rho-Q or increased cortex actin polymerization and cell surface adhesion in response to Rac-Q were similar in control and vMIA-expressing

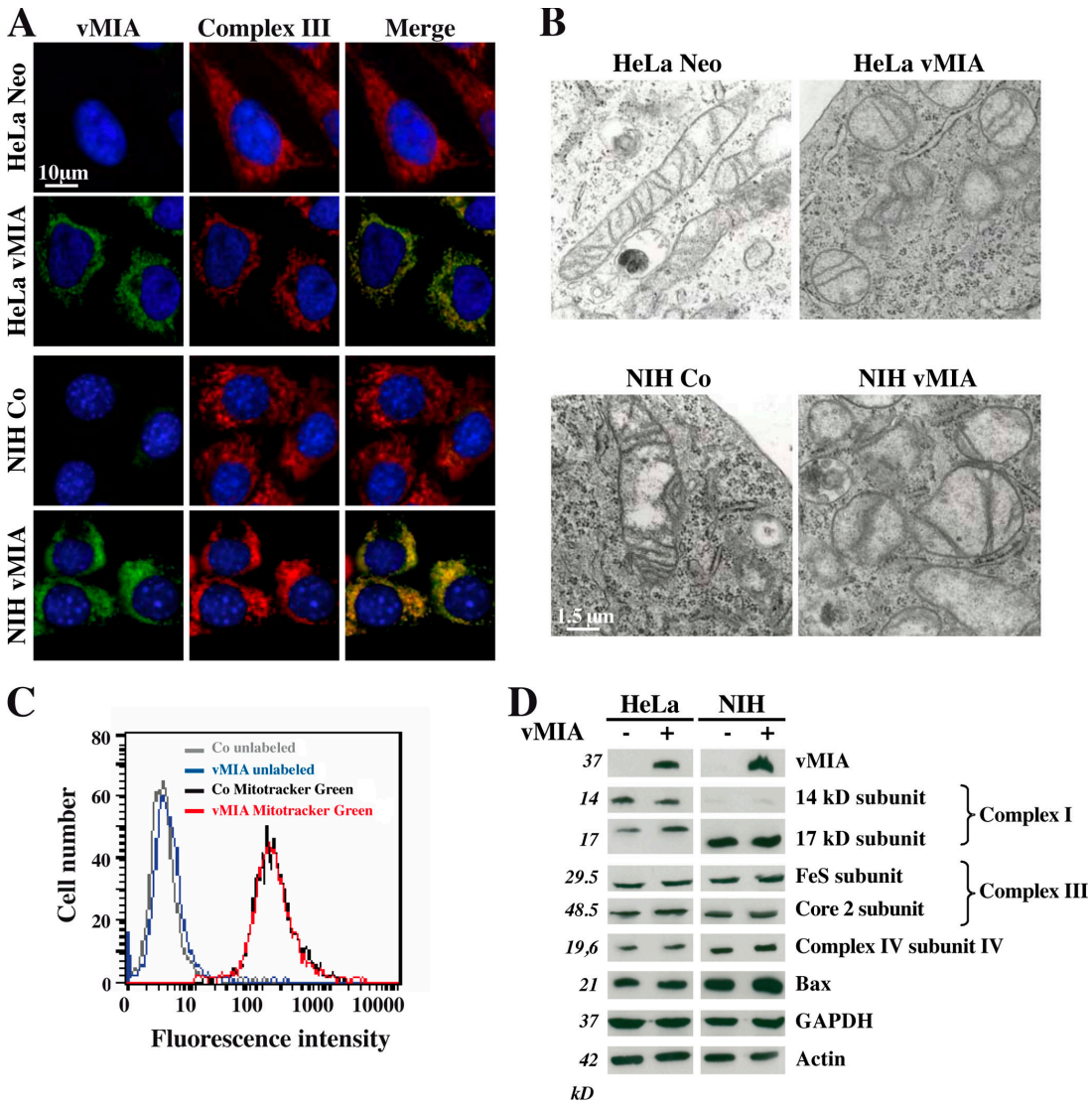

Figure 1. **Mitochondrial morphological changes in cells expressing vMIA.** (A) Immunofluorescence stainings. The expression and localization of vMIA were analyzed by costaining of the Myc tag of vMIA and the core 2 subunit of the complex III on HeLa and NIH3T3 cells stably expressing vMIA (HeLa vMIA and NIH vMIA), as well as control cells (HeLa Neo and NIH Co). (B) Transmission electron microscopy of mitochondrion-rich areas from the indicated cell lines. Note the rounding and the disorganization of cristae in vMIA-expressing mitochondria. (C) Quantification of mitochondrial mass by staining with MitoTracker green. After staining, cells were subjected to flow cytometric analyses. (D) Immunoblotting of respiratory chain subunits. Lysates from the different cell lines were subjected to the immunochemical quantitation of the indicated proteins. GAPDH and actin were probed to control for equal loading.

cells (Fig. S4 B). Nonetheless, in qualitative terms, stress fibers were less numerous in vMIA cells than in Neo cells transfected with Rho-Q. Moreover, cortex actin was less polymerized and cell surface adhesion was comparatively reduced in vMIA cells transfected with Rac-Q (Fig. S4 B). Thus, the Rho-GTPase–induced actin polymerization was functional in HeLa vMIA cells, although at a reduced level. No defect in Rho-GTP could be measured in HeLa vMIA cells (Fig. S4 C). Activation of integrins by extracellular matrix components, such as fibronectin or collagen, is a prominent migration inducer upstream of Rho-GTPase proteins (Parsons et al., 2000; DeMali et al., 2003). Both fibronectin and collagen type I improved cortex actin polymerization and lamellipod extension in Neo and vMIA HeLa cells; they also enhanced focal adhesions, as assessed by the relocalization and activating phosphorylation (Y397) of FAK (Fig. S4 D). However, we again noticed that lamellipod extension and cortex actin repolymerization induced by collagen type I or fibronectin was less pronounced in vMIA than in Neo HeLa cells. These experiments suggested that signaling pathways controlling actin polymerization and migration were functional in vMIA HeLa cells, although these cells showed a reduced, delayed, and incomplete actin polymerization. Inhibition of actin disassembly with jasplakinolide completely restored stress fiber polymerization and the adherence surface of vMIA-expressing HeLa cells (Fig. S4 E), indicating that vMIA had no direct catabolic effect on actin.

vMIA-mediated inhibition of mitochondrial ATP generation

Because vMIA-expressing cells exhibited a modified mitochondrial morphology, we tested whether oxidative phosphorylation would be compromised in these cells. No obvious changes in the

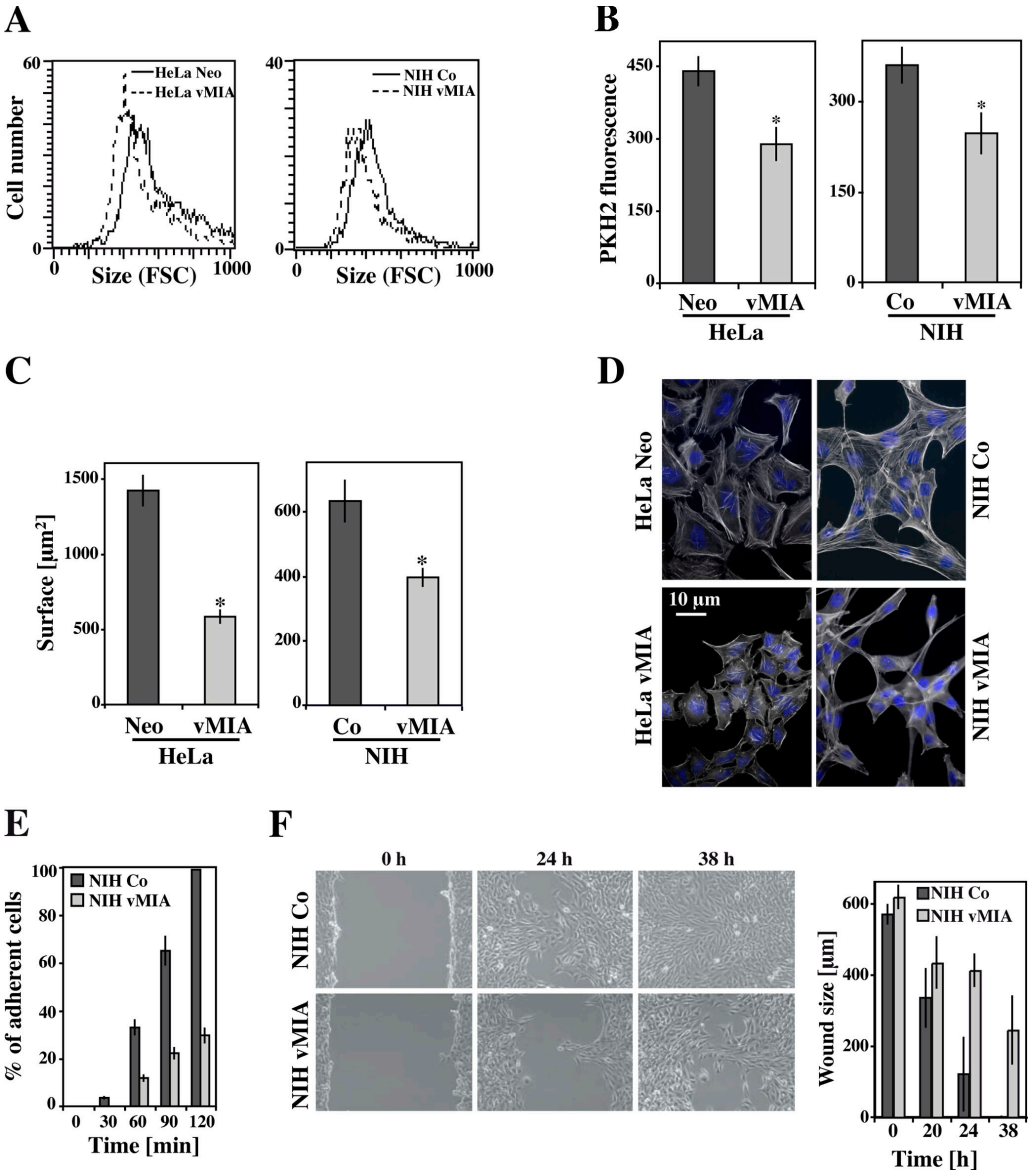

Figure 2. **Effect of vMIA on cell size and the actin cytoskeleton.** (A) Cell size of vMIA-expressing HeLa and NIH cells compared with control cells was determined by cytofluorometric analyses of the FSC. (B) Plasma membrane surface of vMIA-expressing cells. The binding of the green fluorescent dye PKH2-GL to the lipids of the cytoplasmic membrane was measured by cytofluorometry and the mean channel was plotted. $n = 4$. Asterisks represent $P = 0.05$, *t* test. (C) Surface of adherence of vMIA-expressing cells. Cells were stained with CellTracker green, photographed, and subjected to morphometric analyses of the mean surface of adhesion. $n = 2{,}200$ cells. (D) Actin cytoskeleton in vMIA-expressing cells. Control or vMIA-expressing HeLa and NIH cells were stained with phalloidin–Alexa Fluor 568 and Hoechst 33342 to visualize actin and chromatin, respectively. Note the absence of stress fibers and the diminution of the actin cortex induced by vMIA. (E) Adhesion kinetics of vMIA-expressing cells. Cells were trypsinized and allowed to adhere during the indicated period of time, and the percentage of adherent cells was determined by phase-contrast microscopy. $n = 3$. (F) Influence of vMIA on wound healing. The cell monolayer was wounded, and the movement of cells filling the gap was recorded at different times. The mean wound size is plotted. $n = 4$. Error bars represent the mean ± the SD.

composition of respiratory chain complexes of HeLa cells could be detected by two-dimensional (native blue vs. SDS-PAGE) electrophoresis (Fig. S5, available at http://www.jcb.org/cgi/content/full/jcb.200604069/DC1). Polarographic measurements of mitochondrial oxygen consumption indicated that ADP was unable to stimulate the respiratory activity of mitochondria from vMIA-expressing cells. Subsequent blockade of the F_1F_0ATP synthase by oligomycin only poorly decreased oxygen uptake in vMIA-expressing cells (respiratory control [RC] = 1.3), as compared with control (RC = 3.2). The decreased phosphorylating ability of the vMIA-expressing cells was further indicated by the similar effect of the uncoupler CCCP, functionally shunting the F_1F_0ATP synthase on both cell types (RC = 3.3 and 3.4 for vMIA-expressing and control cells, respectively; Fig. 4 A). This result suggested that vMIA compromises the function of the ATP synthasome. The ATP synthasome is a multiprotein ensemble composed of complex V (F_1F_0ATP synthase), ANT, and phosphate inorganic carrier (PiC; Chen et al., 2004). No difference in the abundance of the α-subunit of the F_1F_0ATP synthase was found between vMIA-expressing and control cells, as determined by immunoblotting. Moreover, vMIA-expressing cells and control cells possess a similar F_1F_0ATP synthase activity,

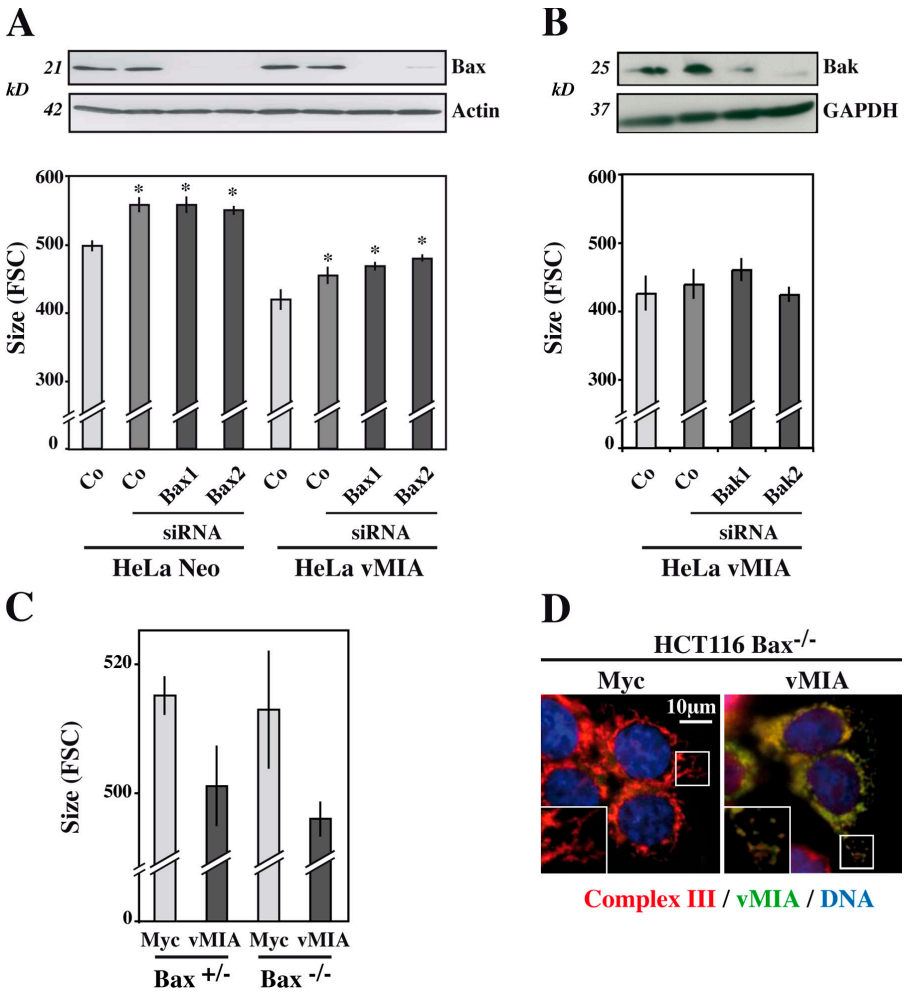

Figure 3. **vMIA-induced morphological changes in Bax-negative cells.** (A) Effect of the Bax knockdown. HeLa Neo or HeLa vMIA cells were transfected with a control siRNA or either of two Bax-specific siRNAs, and the down-regulation of Bax was confirmed by immunoblotting 3 d after transfection. Bax-depleted or control cells were subjected to FACS analysis and the mean size (FSC) was determined. $n = 3$. Asterisks represent $P > 0.05$, *t* test. (B) Effect of the Bak knockdown. HeLa vMIA cells were depleted from Bak with two different siRNAs, and the impact of this manipulation was determined on cell size 2 d after transfection. (C) Impact of vMIA on Bax-deficient HCT116 cells. HCT116 $^{Bax+/-}$ and $^{Bax-/-}$ cells were transfected either with vMIA or Myc control vectors, and cell size was measured by FACS analysis. $n = 3$. (D) vMIA-induced fragmentation of the mitochondrial network in the absence of Bax. The mitochondrial fragmentation was determined by immunofluorescence microscopy after immunostaining of the vMIA Myc tag and the core 2 subunit of complex III in HCT116 $^{Bax-/-}$ cells. Error bars represent the mean ± the SD.

as determined by spectrophotometric assays (Fig. 4 B). vMIA reportedly interacts with mitochondria, particularly with ANT (Goldmacher et al., 1999; Vieira et al., 2001). Hence, we determined the ANT activity on isolated mitochondria in an in vitro assay that does not yield information on the absolute ANT activities, yet allows for the comparison between control and vMIA-expressing cells. vMIA did not compromise the relative ANT activity and rather enhances the uptake of ADP into isolated mitochondria (by a factor of ~2), which can be explained by an increased abundance of ANT protein (Fig. 4 C). Inhibition of the adenylate kinase, using P_1, P_5-Di (adenosine-5′-) pentaphosphate or that of the F_0 part of the ATP synthase by oligomycin, did not abolish the difference in the ADP/ATP exchange rate between mitochondria from control and vMIA-expressing cells, whereas carboxyatractyloside totally inhibited the ANT activity and the ATP efflux measured (unpublished data). The data obtained on ANT activity of isolated mitochondria (Fig. 4 C) were backed up by experiments performed on intact cells (Fig. 4 D). Real-time measurements of the intramatrix ATP levels using permeabilized cells transfected with a mitochondrion-targeted luciferase (Jouaville et al., 1999) revealed that the baseline matrix ATP levels were reduced in vMIA-expressing cells, suggesting defective mitochondrial ATP synthesis. The rate of import of external ATP into the mitochondrial matrix was enhanced in vMIA-expressing cells as compared with control cells (Fig. 4 D). Thus, ANT activity was enhanced by vMIA, much in the way that this has been observed for Bcl-2 overexpression, which also stimulates ANT activity (Belzacq et al., 2003).

Next, we investigated the vMIA effect on the third component of the ATP synthasome, the mitochondrial phosphate carrier. vMIA had no effect on the abundance of the phosphate carrier (Fig. 4 E). However, vMIA reduced the uptake of [^{33}P]phosphate into isolated mitochondria by ~80%, compared with control mitochondria (Fig. 4 E), as determined by an in vitro assay. This observation was confirmed in permeabilized cells that were initially kept in a phosphate-depleted medium, in which ATP synthesis (as detected by matrix- targeted luciferase) was stimulated by the addition of increasing amounts of inorganic phosphate (Fig. 4 F). The phosphate-stimulated ATP generation was reduced in vMIA-expressing cells. Altogether, these data support the notion that vMIA inhibits mitochondrial ATP production, correlating with a decreased activity of the phosphate carrier.

Correlating with the defect in oxidative phosphorylation induced by vMIA (Fig. 4), vMIA-expressing cells exhibited a lower steady-state ATP level, which was ~70% of that in control cells (Fig. 5 A). The ATP levels in cells transfected with a vMIA mutant lacking the mitochondrion-targeting domain

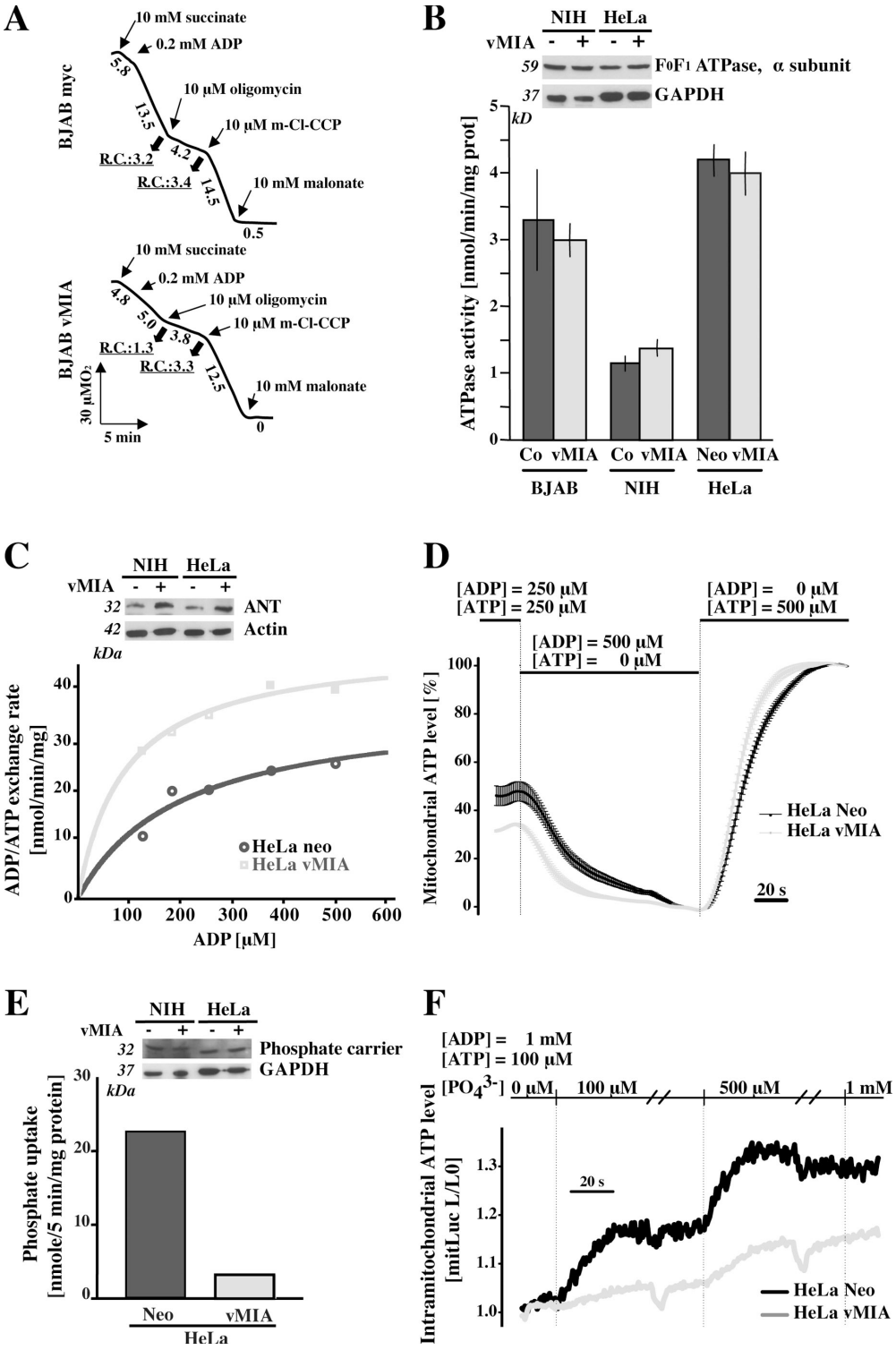

Figure 4. **Effect of vMIA on mitochondrial respiration.** (A) Respiratory control in BJAB cells transfected either with vMIA or the Myc control vector (Myc). Cells were permeabilized, placed in an oxygen electrode, and subjected to the sequential addition of the indicated agents. Note that ADP does not stimulate the oxygen consumption of vMIA-expressing cells, although it does so in control cells. $n = 3$. Similar data were obtained in HeLa cells (not depicted). (B) F_1F_0ATP synthase activity in vMIA-expressing cells. The ATP synthase activity of isolated mitochondria was determined by spectrophotometry, and the abundance of the α subunit was determined by immunoblotting (top). Error bars represent the mean ± the SD. (C) ANT activity in vMIA-expressing mitochondria. Increasing amounts of ADP were added to isolated mitochondria of control and vMIA cells, and the translocase activity of ANT was evaluated as proportional to the $NADP^+$ reduction measured by luminescence assay. Data were fitted with the Michaelis–Menten equation under Kaleidagraph software (Synergy Software). (top) Immunoblot determinations of ANT protein levels. (D) Resting mitochondrial ATP levels and ANT activity in HeLa cells. mtLuc-transfected cells were selectively permeabilized with 25 µM digitonin in an intracellular-like solution that leaves mitochondrial membranes intact. The luciferase activity was monitored to measure the concentration of ATP in the mitochondrial matrix. Before each measurement, cells were pretreated with 5 µM oligomycin for 10 min. The mean ± the SEM of 25 traces are shown in control (black) and vMIA stably transfected (gray) HeLa cells. The ATP/ADP exchange activity of ANT is represented by the kinetics of ATP level after the addition of 500 µM ATP. (E) Phosphate uptake in

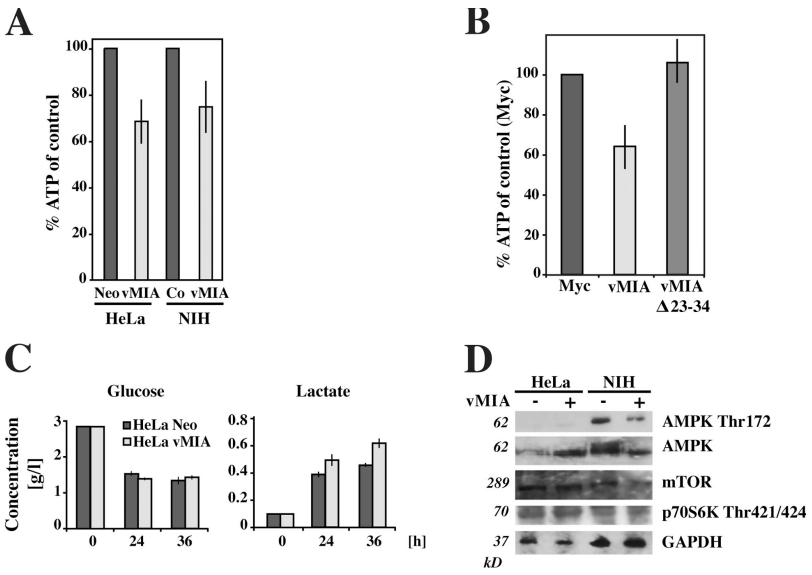

Figure 5. **Metabolic effects of vMIA.** (A) Basic cellular ATP levels in control and vMIA-expressing cell lines. 100% values are set for controls. Error bars represent the mean ± the SD. $n = 6$. (B) Basic cellular ATP levels in Myc (control), vMIA wt, and vMIAΔ23-34–transiently expressing cells. 100% values are set for controls. Representative results are presented. (C) Glucose (left) and lactate concentrations (right) in the medium of vMIA-expressing HeLa cells as compared with normal controls. The measurements were performed in three separate experiments. (D) Effects of vMIA on the phosphorylation of AMPK and $p70^{S6K}$. Immunoblots were probed with antibodies recognizing the indicated phosphoproteins or the proteins as such.

(Δ23-34) (Hayajneh et al., 2001) were similar to that of control cells (Fig. 5 B). Cells expressing vMIA produced more lactate than control cells, indicating that the defect in mitochondrial ATP generation was partially compensated for by an increased anaerobic glycolysis (Fig. 5 C). The partial decrease in ATP induced by vMIA, however, was not sufficient to cause a manifest activation of the AMP kinase (AMPK)–mammalian target of rapamycin (mTOR)–$p70^{S6K}$ kinase pathway, as suggested by the absence of an increased phosphorylation of AMPK and $p70^{S6K}$ kinase in vMIA-expressing cells (Fig. 5 D).

Morphological alterations associated with a cellular ATP defect and a defect in the mitochondrial phosphate carrier

Having established that vMIA-expressing cells had a reduced capacity to generate ATP, we then evaluated the impact of a partial ATP defect on cellular morphology. Exposure of HeLa Neo cells (not depicted) or NIH3T3 control cells to 10 nM oligomycin, which inhibits mitochondrial ATP generation, led to an ∼30% reduction of the intracellular ATP concentration and to a decrease in mean cell size (Fig. 6 A), accompanied by reduced actin polymerization (Fig. 6 B) and a diminished wound healing capacity (Fig. 6 C) similar to that found in vMIA-expressing cells (Fig. 2). Inhibition of the respiratory chain complexes I and II by rotenone and TTFA, respectively, also reduced ATP levels and cell size (Fig. 6 D). Thus, expression of vMIA and exposure of cells to inhibitors of ATP production led to similar morphological changes, suggesting that the effects of vMIA on cellular morphology stem from the vMIA-induced changes in mitochondrial energetics, especially from reduced ATP levels. To formally prove that the defect in the mitochondrial carrier induced by vMIA is responsible for the cytopathic effect, we knocked down the phosphate carrier with two different siRNAs (Fig. 6 E), showing that this manipulation reduced the size of control HeLa cells, yet had no significant effect on the size of HeLa vMIA cells (Fig. 6 F). These data suggest that the effect of vMIA on cell size is secondary to its inhibitory effect on the phosphate carrier.

Cytopathic effects of vMIA during CMV infection

To examine the effects of vMIA in the context of CMV infection, we infected human fibroblasts, which are a cell type permissive for CMV, with either a CMV virus that encodes functional vMIA or with a vMIA-deficient CMV strain. To prevent apoptosis, we used $MRC5^{E1B19k}$ fibroblasts expressing E1B19K, which is a strong cell-death suppressor that has previously been shown to suppress apoptosis induced by vMIA-deficient CMV (Reboredo et al., 2004). $MRC5^{E1B19k}$ cells infected by CMV exhibited a marked rounding-up ∼24 h after infection. This ECE coincided with the onset of strong vMIA expression, as detected by immunofluorescence (Fig. 7, B and C). In contrast, vMIA-deficient CMV, while infecting the cell productively (not depicted), failed to induce ECE, indicating that the observed morphological alteration is truly attributable to vMIA expression (Fig. 7, A–C). In addition to its effects on the global cellular morphology, the expression of vMIA in cells infected with CMV caused a rapid (10 h after infection) fragmentation of the mitochondrial network, from a filamentous to a punctuate pattern, in accordance with previously published data (McCormick et al., 2003). To determine the temporal order between the mitochondrial and the cellular effects of vMIA, we performed confocal microscopy of the vMIA expression in CMV-infected cells, followed by three-dimensional reconstruction of the staining patterns of vMIA and actin. At a first step, vMIA

vMIA-expressing mitochondria compared with control mitochondria, as determined in Materials and methods. Immunoblots show the determination of PiC protein level. (F) Kinetics of phosphate uptake into mitochondria from vMIA-expressing and control HeLa cells. Mitochondrial ATP levels were measured as in D. To ensure maximal activity of the F_1F_0ATP synthase, 1 mM ADP and 100 μM ATP were used in the intracellular buffer. Representative traces from three separate experiments are shown.

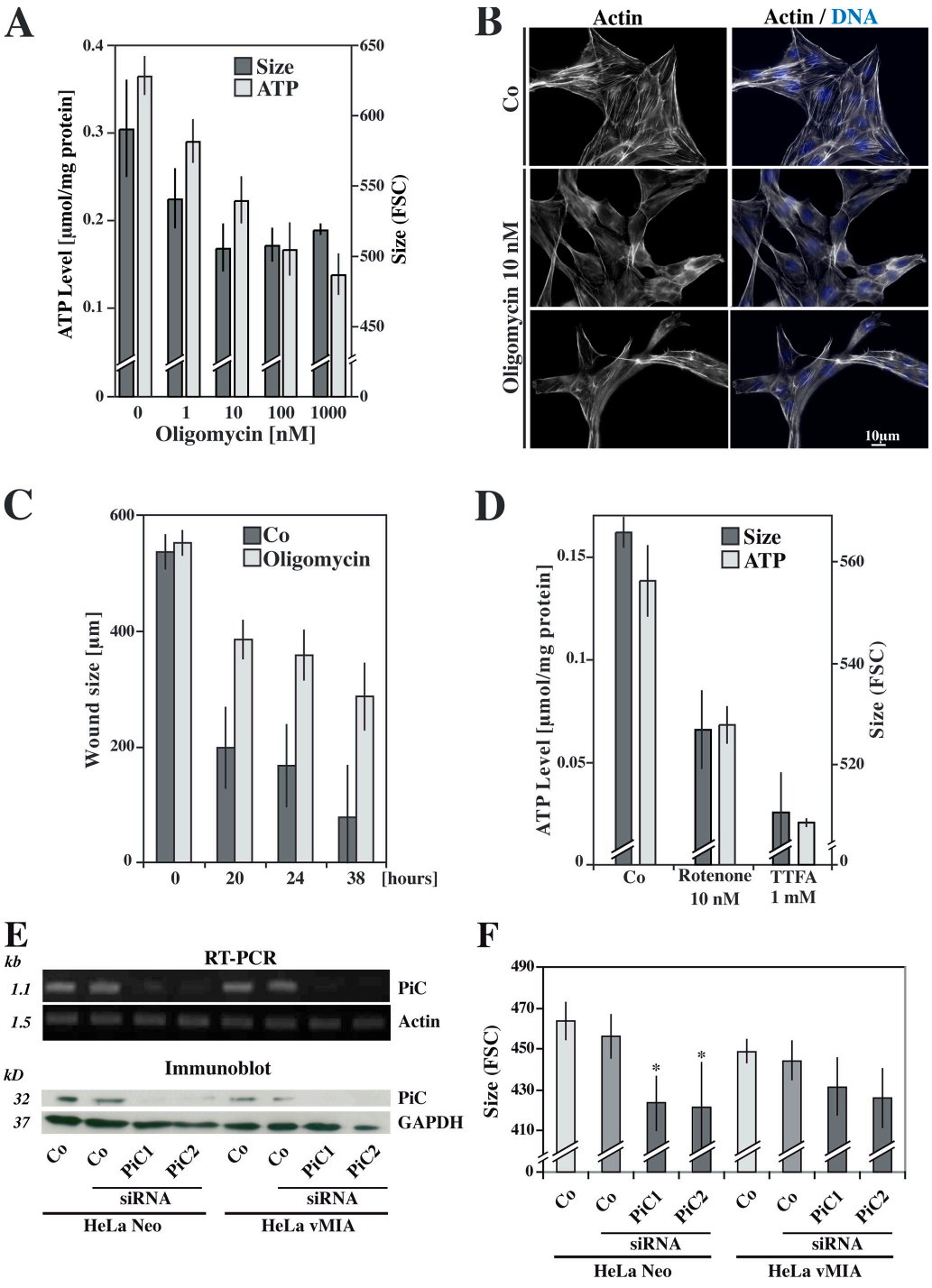

Figure 6. **Effect of ATP depletion on cell size and the actin cytoskeleton.** (A) Impact of ATP depletion on cell size. ATP levels and cell size were determined after 48-h treatment of NIH control cells with increasing doses of oligomycin. Similar results were obtained for HeLa cells (not depicted). (B) Impact of ATP depletion on the actin cytoskeleton. NIH control cells were cultured in the absence or presence of 10 nM oligomycin for 2 d, and then stained to visualize actin and chromatin. Note the reduction of stress fibers, cell size, and adhesion surface. (C) Impact of ATP on wound healing. The NIH control monolayer was wounded, and the size of the gap was evaluated at different times. $n = 3$. (D) Impact of complex I and II inhibition on cell size. Control NIH cells were treated with 10 nM rotenone or 1 mM TTFA for 48 h, and the cellular ATP level and cell size were measured. (E and F) Effect of the depletion of the mitochondrial PiC on cell size. The phosphate carrier was depleted using two distinct siRNAs, and the abundance of the mRNA transcript and the protein levels (E) or cell size (F) were assessed 2 d after transfection. Asterisks indicate significant effects on cell size ($n = 3$) in phosphate carrier–depleted cells, as compared with control transfectants. Error bars represent the mean ± the SD.

was expressed in mitochondria without any major morphological effect. At a second step, vMIA-decorated mitochondria fragmented, while cells conserved a normal shape and a normal actin cytoskeleton. At a final stage, the fragmented mitochondrial network collapsed around the nucleus when cells rounded up (Fig. 7 D). This indicates that the mitochondrial change precedes cytoskeleton alterations and rounding of the cells. The LCE of CMV, nuclear and cytoplasmic granulation, and enlargement

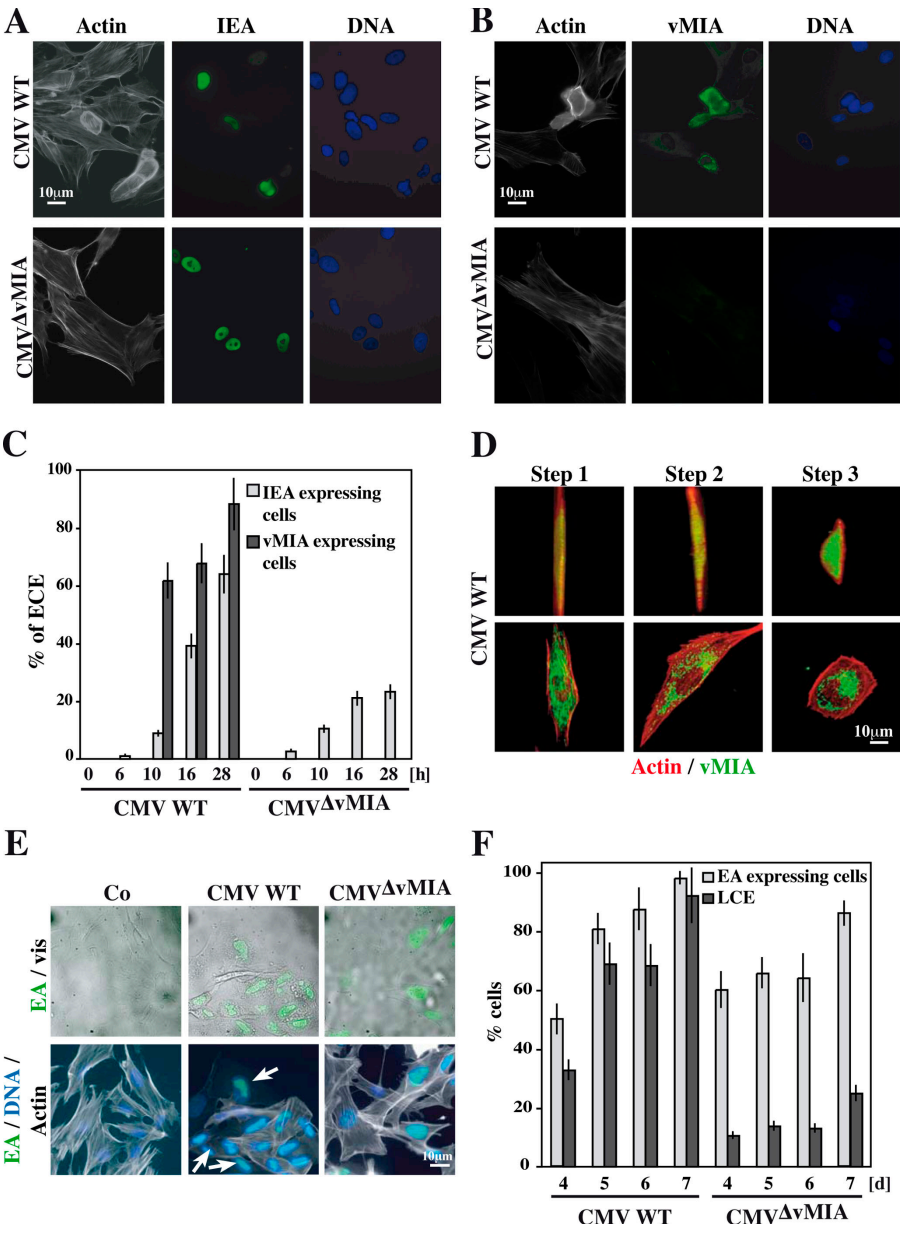

Figure 7. **vMIA-dependent cytopathic effects of CMV.** (A–D) ECE of CMV-encoded vMIA. Human MRC5^{E1B19K} fibroblasts were infected with wild-type (WT) CMV or a vMIA-deficient CMV (ΔvMIA) for the indicated period (28 h in A, B, and D), followed by staining of actin (A, B, and D) and the viral proteins IEA (A) or vMIA (B and D). The percentage of cells exhibiting ECE was determined among the cells expressing IEA or vMIA (C). Confocal immunofluorescence (YX/planar and XZ/vertical views) of wild-type CMV-infected cells was performed, and the three stages of vMIA expression are shown in D; without mitochondrial fragmentation and cell rounding (step 1), with mitochondrial fragmentation and without rounding (step 2), and with fragmentation and rounding (step 3), representing ∼10, ∼2, and ∼88% of the cells, respectively. (E and F) LCE of wild-type (WT) and vMIA-deficient (ΔvMIA) CMV. Human MRC5^{E1B19K} fibroblasts were infected with WT or ΔvMIA CMV for the indicated period (5 d in E; 4–7 d in F), followed by staining of actin and the viral protein EA. Arrows indicate cells with a marked cytopathic effect, namely, granulation and near-to-completed disappearance of the actin cytoskeleton (E). The percentage of cells expressing EA was quantified and the percentage of cells exhibiting LCE was determined among the cells expressing EA (F). Typical results representative of three independent experiments are shown. Error bars represent the mean ± the SD.

of infected cells, associated with a complete loss of phalloidin-detectable actin polymers, was observed 5 d after infection (Fig. 7 E). vMIA was required for the manifestation of LCE because infection with a vMIA-deficient CMV strain failed to induce granulation and actin depolymerization (Fig. 7 F). Altogether, these data demonstrated a major contribution of vMIA to the pathognomonic cytopathic effects of CMV.

Discussion

vMIA is a CMV-derived protein endowed with the capacity of disabling apoptosis through inhibiting Bax-mediated MOMP. We unraveled a hitherto unexpected effect of vMIA that affects mitochondrial bioenergetics and, hence, multiple cellular functions, including shape, size, adhesion, and mobility.

vMIA possesses some functional similarities with Bcl-2 (or Bcl-X_L), yet exhibits important differences in respect to this family of endogenous apoptosis inhibitors. Both vMIA and Bcl-2 act on mitochondria to inhibit MOMP (Susin et al., 1996; Kluck et al., 1997; Yang et al., 1997) and diversion of these proteins to other subcellular localization largely reduces their antiapoptotic potential (Zhu et al., 1996; Goldmacher et al., 1999; Hayajneh et al., 2001). Both vMIA and Bcl-2 reportedly interact with ANT (Marzo et al., 1998; Goldmacher et al., 1999), and both enhance the antiporter activity of ANT (Belzacq et al., 2003; this study). This correlates with the observation that Bcl-2 and Bcl-X_L inhibit the pore-forming function of ANT, while enhancing ATP exchange on the membranes of isolated mitochondria (Vander Heiden et al., 1999, 2001; Belzacq et al., 2003). Similarly, the antiapoptotic function of vMIA has been correlated with a reduced permeabilization of mitochondrial membranes, through an effect on either ANT (Belzacq et al., 2001; Goldmacher et al., 1999) or Bax (Arnoult et al., 2004; Poncet et al., 2004). In contrast to Bcl-2, vMIA partially reduces cellular ATP levels.

Moreover, Bcl-2 has no effects on mitochondrial dynamics and cell size, whereas vMIA causes fragmentation of the mitochondrial network and cell size reduction. Thus, paradoxically, vMIA behaves like Bax or t-Bid, which can fragment mitochondria during apoptosis induction (Nechushtan et al., 2001; Karbowski et al., 2002; Lucken-Ardjomande and Martinou, 2005; Perfettini et al., 2005). Nonetheless, the effect of vMIA on cellular bioenergetics is independent of its interaction with Bax because Bax-negative cells still manifest the mitochondrial fragmentation and bioenergetic effects induced by vMIA. Importantly, vMIA compromises the function of the phosphate carrier, which is the mitochondrial inner membrane protein that exchanges phosphate anions by hydroxyl anions and that oligomerizes with ANT (and the F_1F_0ATP synthase) within the so-called ATP synthasome. This structure generates ATP within the matrix, while guaranteeing for its export (which is limited by the import of its precursors, i.e., ADP and inorganic phosphate). Thus, a strong inhibition of phosphate carrier activity by vMIA can limit the generation of ATP in the matrix and cause a bioenergetic deficiency in the entire cell. How vMIA (which is located in the mitochondrial outer membrane) affects the function of the phosphate carrier (in the inner mitochondrial membrane) remains a conundrum. However, it has been found that proteins that are located in the inner membrane can interact with outer membrane proteins within contact sites, and allosteric effects across the two membranes have been documented (Crompton, 2003; Halestrap and Brennerb, 2003; Machida et al., 2006).

One plausible explanation of the findings obtained in this paper is portrayed in the following scenario. Upon CMV infection, the UL37 exon 1 is transcribed and translated into vMIA protein, which is imported into mitochondria, where it interacts with the ATP synthasome, reducing the enzymatic activity of the phosphate carrier. This ultimately causes a reduction in mitochondrial ATP production and, hence, whole ATP levels. By analogy with other inhibitors of mitochondrial respiration that induce reversible mitochondrial fragmentation without apoptosis induction (Legros et al., 2002; Ishihara et al., 2003), vMIA induces mitochondrial fission. On theoretical grounds, the disruption of the mitochondrial network could be caused by either ATP depletion or the effects on mitochondrial proteins. Thus, reduced ATP levels can inhibit mitofusin-1–dependent fusion without affecting Drp1-dependent fission, causing mitochondrial fragmentation as the net result (Legros et al., 2002). Moreover, the antiretroviral drug nelfinavir, which affects ANT structure (Weaver et al., 2005), can induce mitochondrial fragmentation without reducing ATP levels (Perfettini et al., 2005; Roumier et al., 2005). Thus, it is not clear whether the vMIA-induced ATP depletion or the vMIA interaction with the ATP synthasome accounts for the alteration of mitochondrial dynamics. Shortly after mitochondrial fission, cells manifest rounding-up and accumulate a series of alterations that are similarly induced by vMIA expression or ATP depletion, namely a reduction in cell size, adhesion, and mobility. These changes correlate with a depolymerization of stress fibers and a reduced actin cortex, two changes that are not secondary to alterations in Rho or Rac signaling. Although ATP and GTP levels may be expected to correlate (Dagher, 2000), no detectable defect in Rho-GTP levels was induced by vMIA. Previous studies have unraveled the deleterious effects of ATP depletion on the actin cytoskeleton, resulting in lamellipod retraction, stress fiber collapse, and ventral F-actin aggregation, e.g., in conditions of ischemia (Ganote and Armstrong, 1993; Shelden et al., 2002; Atkinson et al., 2004). Hence, the effects induced by vMIA on the cytoskeleton are likely to be fully explained by ATP depletion.

At first glance, it appears counterintuitive that a virus might be "interested" in reducing ATP levels, which might compromise cellular functions and, hence, reduce viral replication. Indeed, herpesviridae other than CMV encode apoptosis-inhibitory proteins with a marked homology to Bcl-2. This applies, for example, to two nononcogenic herpesviruses (Herpesvirus Saimiri and Herpesvirus 68), as well as to two oncogenic viruses, namely, Kaposi's sarcoma associates herpesvirus and Epstein Barr virus (Cuconati and White, 2002; Hardwick and Bellows, 2003; Boya et al., 2004). Transfection of the two Epstein Barr virus Bcl-2 homologues, BALF or BHRF1, has no measurable effect on mitochondrial or cellular morphology (unpublished data), indicating that they act like endogenous Bcl-2. As a matter of speculation, a partial reduction of ATP levels, by ~30%, might be "useful" for CMV. As a possibility, actin depolymerization might facilitate the anterograde and retrograde traffic of viral particles and products throughout the CMV life cycle, as has been suggested previously (Jones et al., 1986; Cudmore and Reckmann, 1997; Ploubidou and Way, 2001; Dohner and Sodeik, 2005). Moreover, reduced adhesion or migration of CMV-infected cells might participate in the theratogenic effects of CMV, e.g., on the fetal brain (Shinmura et al., 1997).

Among the β-herpesviridae, CMV is characterized by a long life cycle (4–5 d) and a peculiar cytopathic effect, which is observable on many different CMV-infectable cell types (Kowalik et al., 1994; Warren et al., 1994). This characteristic cytopathic effect shaped the name of the virus. The data reported in this study provide a molecular explanation for the cytopathic effect of CMV, which can be attributed to the expression of one single viral protein, vMIA.

Materials and methods

Cell culture, transfection, CMV infection, and treatment

HeLa and BJAB vMIA-expressing cells were previously described (Goldmacher et al., 1999). NIH3T3 cells were stably transfected with pLncx/vMIAmyc, coding for vMIA-Myc (provided by F. Subra, Ecole Normale Supérieure, Cachan, France). MRC5 human fibroblasts stably expressing E1B19K protein ($MRC5^{E1B19K}$) were infected with vMIA-deficient CMV ($CMV^{\Delta vMIA}$) or its parental strain, AD169*var*ATCC (CMV WT; Reboredo et al., 2004). $HCT116^{Bax-/-}$ cells were provided by B. Vogelstein (Johns Hopkins University, Baltimore, MD; Zhang et al., 2000). MRC5, HeLa, BJAB, and HCT116 were cultured as previously described (Poncet et al., 2004). NIH3T3 cells were cultured in DME supplemented with 10% newborn calf serum. To knock down Bax, Bak, or PiC expression, two siRNAs were used (hBax-384 for Bax1, hBax-208 for Bax2, hBak01-258 for Bak1, [Perfettini et al., 2004] Qiagen hp_Bak_1_5 for Bak2; and sense strands CUGGCGCACAUCACUAUAU and CCAGGUUAUGCCAACACUU for PiC1 and PiC2, respectively). As a control, siRNA luciferase (Proligo, siRNA luc) was used. 0.5 μl Oligofectamine (Invitrogen) and 30 pmol siRNA were added to a 24-well plate. Plasmid transfections were performed in a 6-well plates using Lipofectamine (Invitrogen) at a ratio of 3 μg Lipofectamine for 2 μg plasmid. NIH3T3 cells were treated with oligomycin, TTFA, and rotenone (Sigma-Aldrich).

Cytofluorometry and microscopy

Cells were incubated for 15 min at 37°C with 150 nM MitoTracker green (Invitrogen). The cell size was quantified as the forward scatter channel (FSC). Plasma membranes were labeled with the PKH2 Green Fluorescent Cell Linker kit (Sigma-Aldrich). Immunofluorescence experiments were performed as previously described (Castedo et al., 2002). vMIA Myc-tag, actin filaments, and DNA were visualized using Myc-FITC (Abcam), Alexa Fluor 568 phalloidin (Invitrogen), and Hoechst 33342 (Invitrogen). The primary antibodies used were as follows: vMIA (Goldmacher et al., 1999), immediate early antigen (IEA), early antigen (EA; Argene), and complex III core 2 (Invitrogen). Secondary Alexa Fluor–coupled antibodies were obtained from Invitrogen. In most experiments, a Leica DMIR2 inverted fluorescence microscope (camera DFC300FX, acquisition software Leica FW4000) was used. For adhesion assay, cells were trypsinized and seeded on Nunc culture dishes. Alternatively, cells were grown to confluence and the monolayer was wounded by scratching with a pipette tip. Photographs were taken with visible light at 10×. To calculate the cell surface area, cells cultured on polystyrene dishes were labeled for 40 min with 1 μM CellTracker green (Invitrogen) and washed, and then photographs were taken in 10 areas at 10× (LSM510 confocal microscope; Carl Zeiss MicroImaging, Inc; and ImageJ software; National Institutes of Health). Cells infected with CMV were examined with a LSM510, using LSM Image Browser (Carl Zeiss MicroImaging, Inc.. Transmission electron microscopy was performed as previously described (Boya et al., 2005).

Bioenergetic methods

ATP was measured with the bioluminescence assay kit HS-II (Roche). Polarographic studies performed on BJAB cells were performed as previously described (Rustin et al., 1994). The RC was calculated by dividing oxygen consumption before and after addition of ADP/ATP. The oligomycin-sensitive F_1F_0ATP synthase activity was measured using the spectrophotometric-coupled assay with pyruvate kinase and lactic dehydrogenase (Rustin et al., 1994). To measure ANT activity in vitro, mitochondria were isolated from Neo and vMIA HeLa cells by differential centrifugation in 0.3 M sucrose buffer at 4°C. The ADP/ATP exchange rates of the two types of mitochondria were concomitantly evaluated on the equivalent of 75-μg mitochondrial proteins in a 96-multiwell plate. ATP efflux induced by externally added ADP was monitored by following NADP+ reduction, as previously described (Passarella et al., 1988). This assay was validated for microtiter plate format analysis and found to produce results similar to the radiolabeled-ATP–based assay (Belzacq et al., 2003). For determination of phosphate carrier activity (Palmieri and Klingenberg, 1979), mitochondria from HeLa cells were isolated using a mitochondrial isolation kit (Pierce Chemical, Co.). 1 mM [^{33}P]phosphate was added to 60 μg mitochondria suspended in 250 mM sucrose, 1 mM EDTA, and 10 mM Tris-HCl, pH 7.4, in a final volume of 110 μl at 25°C. The reaction was terminated after 5 min by addition of 1 mM mersalyl (Sigma-Aldrich). D-Glucose and L-Lactic acid amounts in cell culture media were calculated by the UV method, with enzymatic kits (Boehringer Mannheim/R-Biopharm). To measure the mitochondrial ATP levels in vivo, HeLa cells seeded on glass coverslips were transfected with 3 μg mitochondrially targeted luciferase (Jouaville et al., 1999). 36 h later, cells were transferred to a custom-built luminometer perfusion chamber (Rizzuto et al., 1998). The plasma membrane was selectively permeabilized with 25 μM digitonin for 1 min, and cells were suspended in an intracellular-like buffer (130 mM KCl, 10 mM NaCl, 1 mM $MgSO_4$, 5 mM succinate, 0.5 mM K_2HPO_4, 20 mM Hepes, pH 7.0, 1 mM EGTA, and 130 μM $CaCl_2$, giving a free [Ca^{2+}] of 100 nM) at 37°C. Before addition of 20 μM luciferin, ATP, and ADP, cells were treated for 10 min with 5 μM oligomycin. Traces were normalized to the minimal and maximal luminescence levels obtained in the 500 μM ADP/no ATP and no ADP/500 μM ATP solutions, respectively. To measure phosphate dependency, cells were perfused consecutively with 0, 0.1, 0.5, and 1 mM $H_2PO_4^-$ in conditions of maximal activity of the F_1F_0 ATP synthase (obtained by addition of 1 mM ADP and 100 μM ATP).

Immunoblotting

Cells were lysed in 0.1% SDS-PBS buffer and spun for 5 min at 15,000 *g*. 25 μg total protein were separated by SDS-PAGE. The primary antibodies used were as follows: Myc 9E10 (Santa Cruz Biotechnology, Inc.), Bax N-ter (Millipore), GAPDH, actin (CHEMICON International, Inc.), and PiC (Fiermonte et al., 1998). All antibodies specific for OXPHOS subunits were obtained from Invitrogen. Antibodies for mTOR, AMPK, and p70S6K were purchased from Cell Signaling Technology. Secondary HRP conjugated antibodies were obtained from Southern Biotechnologies.

Online supplemental material

Fig. S1 shows the cell cycle independence of cell size reduction induced by vMIA. Fig. S2 shows cell type–specific apoptosis inhibition by vMIA. Fig. S3 shows the effect of the cell culture substrates on cell size. Fig. S4 shows the effects of Rho and Rac GTPases (provided by C. Lamaze, Curie Institute, Paris, France), cell culture substrates on the actin cytoskeleton, and focal adhesion. Fig. S5 shows two-dimensional gel electrophoresis of respiratory chain complexes from control and vMIA-expressing mitochondria. Online supplemental material is available at http://www.jcb.org/cgi/content/full/jcb.200604069/DC1.

We thank Drs. Christophe Lamaze for Rho and Rac plasmids, Frédéric Subra for NIH3T3 cells expressing vMIA, and Richard Greaves and Bernt Vogelstein for Bax-deficient HCT116 cells.

G. Kroemer is supported by Ligue Nationale Contre le Cancer, European Community (Active p53 and RIGHT), and Sidaction.

Submitted: 12 April 2006
Accepted: 22 August 2006

References

Arnoult, D., L.M. Bartle, A. Skaletskaya, D. Poncet, N. Zamzami, P.U. Park, J. Sharpe, R.J. Youle, and V.S. Goldmacher. 2004. Cytomegalovirus cell death suppressor vMIA blocks Bax- but not Bak-mediated apoptosis by binding and sequestering Bax at mitochondria. *Proc. Natl. Acad. Sci. USA*. 101:7988–7989.

Atkinson, S.J., M.A. Hosford, and B.A. Molitoris. 2004. Mechanism of actin polymerization in cellular ATP depletion. *J. Biol. Chem.* 279:5194–5199.

Belzacq, A.S., C. El Hamel, H.L.A. Vieira, I. Cohen, D. Haouzi, D. Metivier, P. Marchetti, V. Goldmacher, C. Brenner, and G. Kroemer. 2001. The adenine nucleotide translocator mediates the mitochondrial membrane permeabilization induced by lonidamine, arsenite and CD437. *Oncogene*. 20:7579–7587.

Belzacq, A.S., H.L. Vieira, F. Verrier, G. Vandecasteele, I. Cohen, M.C. Prevost, P.X. Petit, A. Kahn, B. Roques, R. Rizzuto, et al. 2003. Bcl-2 and Bax modulate adenine nucleotide translocase activity. *Cancer Res.* 63:541–546.

Boya, P., B. Roques, and G. Kroemer. 2001. Bacterial and viral proteins regulating apoptosis at the mitochondrial level. *EMBO J.* 20:4325–4331.

Boya, P., K. Andreau, D. Poncet, N. Zamzami, J.-L. Perfettini, D. Metivier, D.M. Ojcius, M. Jaattela, and G. Kroemer. 2003. Lysosomal membrane permeabilization induces cell death in a mitochondrion-dependent fashion. *J. Exp. Med.* 197:1323–1334.

Boya, P., A.L. Pauleau, D. Poncet, R.A. Gonzalez-Polo, N. Zamzami, and G. Kroemer. 2004. Viral proteins targeting mitochondria: controlling cell death. *Biochim. Biophys. Acta*. 1659:178–189.

Boya, P., R.-A. Gonzalez-Polo, N. Casares, J.-L. Perfettini, P. Dessen, N. Larochette, D. Metivier, D. Meley, S. Souquere, G. Pierron, et al. 2005. Inhibition of macroautophagy triggers apoptosis. *Mol. Cell. Biol.* 25:1025–1040.

Castedo, M., T. Roumier, J. Blanco, K.F. Ferri, J. Barretina, K. Andreau, J.-L. Perfettini, A. Armendola, R. Nardacci, P. LeDuc, et al. 2002. Sequential involvement of Cdk1, mTOR and p53 in apoptosis induced by the human immunodeficiency virus-1 envelope. *EMBO J.* 21:4070–4080.

Chen, C., Y. Ko, M. Delannoy, S.J. Ludtke, W. Chiu, and P.L. Pedersen. 2004. Mitochondrial ATP synthasome: three-dimensional structure by electron microscopy of the ATP synthase in complex formation with carriers for Pi and ADP/ATP. *J. Biol. Chem.* 279:31761–31768.

Chiou, S.H., J.H. Liu, S.S. Chen, W.T. Liu, J.C. Lin, W.W. Wong, W.S. Tseng, C.K. Chou, C.Y. Liu, L.L. Ho, and W.M. Hsu. 2002. Apoptosis of human retina and retinal pigment cells induced by human cytomegalovirus infection. *Ophthalmic Res.* 34:77–82.

Crompton, M. 2003. On the involvement of mitochondrial intermembrane junctional complexes in apoptosis. *Curr. Med. Chem.* 10:1473–1484.

Cuconati, A., and E. White. 2002. Viral homologs of BCL-2: role of apoptosis in the regulation of virus infection. *Genes Dev.* 16:2465–2478.

Cudmore, S., and I. Reckmann. 1997. Viral manipulations of the actin cytoskeleton. *Trends Microbiol.* 5:142–148.

Dagher, P.C. 2000. Modeling ischemia in vitro: selective depletion of adenine and guanine nucleotide pools. *Am. J. Physiol. Cell Physiol.* 279: C1270–C1277.

DeBiasi, R.L., B.K. Kleinschmidt-DeMasters, S. Richardson-Burns, and K.L. Tyler. 2002. Central nervous system apoptosis in human herpes simplex virus and cytomegalovirus encephalitis. *J. Infect. Dis.* 186:1547–1557.

DeMali, K.A., K. Wennerberg, and K. Burridge. 2003. Integrin signaling to the actin cytoskeleton. *Curr. Opin. Cell Biol.* 15:572–582.

Dohner, K., and B. Sodeik. 2005. The role of the cytoskeleton during viral infection. *Curr. Top. Microbiol. Immunol.* 285:67–108.

Fiermonte, G., V. Dolce, and F. Palmieri. 1998. Expression in *Escherichia coli*, functional characterization, and tissue distribution of isoforms A and B of the phosphate carrier from bovine mitochondria. *J. Biol. Chem.* 273:22782–22787.

Gandhi, M.K., and R. Khanna. 2004. Human cytomegalovirus: clinical aspects, immune regulation, and emerging treatments. *Lancet Infect. Dis.* 4:725–738.

Ganote, C., and S. Armstrong. 1993. Ischaemia and the myocyte cytoskeleton: review and speculation. *Cardiovasc. Res.* 27:1387–1403.

Goldmacher, V.S. 2005. Cell death suppression by cytomegaloviruses. *Apoptosis*. 10:251–265.

Goldmacher, V.S., L.M. Bartle, S. Skletskaya, C.A. Dionne, N.L. Kedersha, C.A. Vater, J.W. Han, R.J. Lutz, S. Watanabe, E.D.C. McFarland, et al. 1999. A cytomegalovirus-encoded mitochondria-localized inhibitor of apoptosis structurally unrelated to Bcl-2. *Proc. Natl. Acad. Sci. USA*. 96:12536–12541.

Halestrap, A.P., and C. Brennerb. 2003. The adenine nucleotide translocase: a central component of the mitochondrial permeability transition pore and key player in cell death. *Curr. Med. Chem.* 10:1507–1525.

Hardwick, J.M., and D.S. Bellows. 2003. Viral versus cellular BCL-2 proteins. *Cell Death Differ.* 10:S68–S76.

Hayajneh, W.A., A.M. Colberg-Oley, A. Skaleskaya, L.M. Bartle, M.M. Lesperance, D.G. Contopoulos-Ionnidis, N.L. Kedersha, and V.S. Goldmacher. 2001. The sequence and antiapoptotic functional domains of the human cytomegalovirus UL37 exon 1 immediate early protein are conserved in multiple primary strains. *Virology*. 279:233–240.

Ishihara, N., A. Jofuku, Y. Eura, and K. Mihara. 2003. Regulation of mitochondrial morphology by membrane potential, and DRP1-dependent division and FZO1-dependent fusion reaction in mammalian cells. *Biochem. Biophys. Res. Commun.* 301:891–898.

Jones, N.L., J.C. Lewis, and B.A. Kilpatrick. 1986. Cytoskeletal disruption during human cytomegalovirus infection of human lung fibroblasts. *Eur. J. Cell Biol.* 41:304–312.

Jouaville, L.S., P. Pinton, C. Bastianutto, G.A. Rutter, and R. Rizzuto. 1999. Regulation of mitochondrial ATP synthesis by calcium: evidence for a long-term metabolic priming. *Proc. Natl. Acad. Sci. USA*. 96:13807–13812.

Karbowski, M., Y.J. Lee, B. Gaume, S.Y. Jeong, S. Frank, A. Nechushtan, A. Santel, M. Fuller, C.L. Smith, and R.J. Youle. 2002. Spatial and temporal association of Bax with mitochondrial fission sites, Drp1, and Mfn2 during apoptosis. *J. Cell Biol.* 159:931–938.

Kluck, R.M., E. Bossy-Wetzel, D.R. Green, and D.D. Newmeyer. 1997. The release of cytochrome *c* from mitochondria: a primary site for Bcl-2 regulation of apoptosis. *Science*. 275:1132–1136.

Kowalik, T.F., A.D. Yurochko, C.A. Rinehart, C.V. Lee, and E.S. Huang. 1994. Productive infection of human endometrial stromal cells by human cytomegalovirus. *Virology*. 202:247–257.

Legros, F., A. Lombes, P. Frachon, and M. Rojo. 2002. Mitochondrial fusion in human cells is efficient, requires the inner membrane potential, and is mediated by mitofusins. *Mol. Biol. Cell.* 13:4343–4354.

Lucken-Ardjomande, S., and J.C. Martinou. 2005. Newcomers in the process of mitochondrial permeabilization. *J. Cell Sci.* 118:473–483.

Machida, K., Y. Ohta, and H. Osada. 2006. Suppression of apoptosis by cyclophilin D via stabilization of hexokinase II mitochondrial binding in cancer cells. *J. Biol. Chem.* 281:14314–14320.

Marzo, I., C. Brenner, N. Zamzami, J. Jürgensmeier, S.A. Susin, H.L.A. Vieira, M.-C. Prévost, Z. Xie, S. Matsuyama, J.C. Reed, and G. Kroemer. 1998. Bax and adenine nucleotide translocator cooperate in the mitochondrial control of apoptosis. *Science*. 281:2027–2031.

McCormick, A.L., V.L. Smith, D. Chow, and E.S. Mocarski. 2003. Disruption of mitochondrial networks by the human cytomegalovirus UL37 gene product viral mitochondrion-localized inhibitor of apoptosis. *J. Virol.* 77:631–641.

Nechushtan, A., C.L. Smith, I. Lamensdorf, S.H. Yoon, and R.J. Youle. 2001. Bax and Bak coalesce into novel mitochondria-associated clusters during apoptosis. *J. Cell Biol.* 153:1265–1276.

Palmieri, F. 2004. The mitochondrial transporter family (SLC25): physiological and pathological implications. *Pflugers Arch.* 447:689–709.

Palmieri, F., and M. Klingenberg. 1979. Direct methods for measuring metabolite transport and distribution in mitochondria. *Methods Enzymol.* 56:279–301.

Parsons, J.T., K.H. Martin, J.K. Slack, J.M. Taylor, and S.A. Weed. 2000. Focal adhesion kinase: a regulator of focal adhesion dynamics and cell movement. *Oncogene*. 19:5606–5613.

Passarella, S., A. Ostuni, A. Atlante, and E. Quagliariello. 1988. Increase in the ADP/ATP exchange in rat liver mitochondria irradiated in vitro by helium-neon laser. *Biochem. Biophys. Res. Commun.* 156(2):978–986.

Perfettini, J.-L., T. Roumier, M. Castedo, N. Larochette, P. Boya, B. Reynal, V. Lazar, F. Ciccosanti, R. Nardacci, J.M. Penninger, et al. 2004. NF-kB and p53 are the dominant apoptosis-inducing transcription factors elicited by the HIV-1 envelope. *J. Exp. Med.* 199:629–640.

Perfettini, J.-L., T. Roumier, and G. Kroemer. 2005. Mitochondrial fusion and fission in the control of apoptosis. *Trends Cell Biol.* 15:179–183.

Ploubidou, A., and M. Way. 2001. Viral transport and the cytoskeleton. *Curr. Opin. Cell Biol.* 13:97–105.

Poncet, D., P. Boya, N. Larochette, A.-A. Jalil, A.-L. Paulau, P.-F. Cartron, F.M. Vallette, C. Schnebelen, L.M. Bartle, A. Skaleskaya, et al. 2004. An anti-apoptotic viral protein that recruits Bax to mitochondria. *J. Biol. Chem.* 279:22605–22614.

Raftopoulou, M., and A. Hall. 2004. Cell migration: Rho GTPases lead the way. *Dev. Biol.* 265:23–32.

Reboredo, M., R.F. Greaves, and G. Hahn. 2004. Human cytomegalovirus proteins encoded by UL37 exon 1 protect infected fibroblasts against virus-induced apoptosis and are required for efficient virus replication. *J. Gen. Virol.* 85:3555–3567.

Ridley, A.J. 2001. Rho GTPases and cell migration. *J. Cell Sci.* 114:2713–2722.

Rizzuto, R., P. Pinton, W. Carrington, F.S. Fay, K.E. Fogarty, L.M. Lifshitz, R.A. Tuft, and T. Pozzan. 1998. Close contacts with the endoplasmic reticulum as determinants of mitochondrial Ca2+ responses. *Science*. 280:1763–1766.

Roumier, T., G. Szabadkai, A.M. Simoni, J.-L. Perfettini, A.-L. Paulau, M. Castedo, D. Metivier, A. Badley, C.D. Rizzuto, and G. Kroemer. 2005. HIV-1 protease inhibitors and cytomegalovirus vMIA induce mitochondrial fragmentation without triggering apoptosis. *Cell Death Differ.* 12:91–93.

Rustin, P., D. Chretien, T. Bourgeron, B. Gerard, A. Rotig, J.M. Saudubray, and A. Munnich. 1994. Biochemical and molecular investigations in respiratory chain deficiencies. *Clin. Chim. Acta*. 228:35–51.

Sekhon, H.S., R.D. Press, W.A. Schmidt, M. Hawley, and A. Rader. 2004. Identification of cytomegalovirus in a liquid-based gynecologic sample using morphology, immunohistochemistry, and DNA real-time PCR detection. *Diagn. Cytopathol.* 30:411–417.

Shelden, E.A., J.M. Weinberg, D.R. Sorenson, C.A. Edwards, and F.M. Pollock. 2002. Site-specific alteration of actin assembly visualized in living renal epithelial cells during ATP depletion. *J. Am. Soc. Nephrol.* 13:2667–2680.

Shinmura, Y., I. Kosugi, S. Aiba-Masago, S. Baba, L.R. Yong, and Y. Tsutsui. 1997. Disordered migration and loss of virus-infected neuronal cells in developing mouse brains infected with murine cytomegalovirus. *Acta Neuropathol. (Berl.)*. 93:551–557.

Susin, S.A., N. Zamzami, M. Castedo, T. Hirsch, P. Marchetti, A. Macho, E. Daugas, M. Geuskens, and G. Kroemer. 1996. Bcl-2 inhibits the mitochondrial release of an apoptogenic protease. *J. Exp. Med.* 184:1331–1342.

Tzankov, A., G. Stifter, I. Tschorner, G. Gastl, and G. Mikuz. 2003. Detection of apoptoses in gastro-intestinal graft-versus-host disease and cytomegalovirus colitis by a commercially available antibody against caspase-3. *Pathol. Res. Pract.* 199:337–340.

Vander Heiden, M.G., N.S. Chandel, P.T. Schumacker, and C.B. Thompson. 1999. Bcl-xL prevents cell death following growth factor withdrawal by facilitating mitochondrial ATP/ADP exchange. *Mol. Cell*. 3:159–167.

Vander Heiden, M.G., X.X. Li, E. Gottleib, R.B. Hill, C.B. Thompson, and M. Colombini. 2001. Bcl-xL promotes the open configuration of the voltage-dependent anion channel and metabolite passage through the outer mitochondrial membrane. *J. Biol. Chem.* 276:19414–19419.

Vieira, H.L., A.-S. Belzacq, D. Haouzi, F. Bernassola, I. Cohen, E. Jacotot, K.F. Ferri, E.H. Hamel, L.M. Bartle, G. Melino, et al. 2001. The adenine nucleotide translocator: a target of nitric oxide, peroxynitrite and 4-hydroxynonenal. *Oncogene*. 20:4305–4316.

Warren, A.P., C.N. Owens, L.K. Borysiewicz, and K. Patel. 1994. Down-regulation of integrin alpha 1/beta 1 expression and association with cell rounding in human cytomegalovirus-infected fibroblasts. *J. Gen. Virol.* 75:3319–3325.

Weaver, J.G.R., A. Tarze, T.C. Moffa, M. Lebras, A. Deniaud, C. Brenner, G.D. Bren, M.Y. Morin, B.N. Phenix, L. Dong, et al. 2005. Inhibition of adenine nucleotide translocator pore function and protection against apoptosis in vivo by an HIV protease inhibitor. *J. Clin. Invest.* 115:1828–1838.

Yang, J., X. Liu, K. Bhalla, C.N. Kim, A.M. Ibrado, J. Cai, T.-I. Peng, D.P. Jones, and X. Wang. 1997. Prevention of apoptosis by Bcl-2: release of cytochrome c from mitochondria blocked. *Science*. 275:1129–1132.

Zhang, L., J. Yu, B.H. Park, K.W. Kinzler, and B. Vogelstein. 2000. Role of BAX in the apoptotic response to anticancer agents. *Science*. 290:989–992.

Zhu, W., A. Cowie, G.W. Wasfy, L.Z. Penn, B. Leber, and D.W. Andrews. 1996. Bcl-2 mutants with restricted subcellular localization reveal spatially distinct pathways for apoptosis in different cell types. *EMBO J.* 15:4130–4141.